Upwelling of Arctic pycnocline associated with shear motion of sea ice

M. G. McPhee
McPhee Research Company, Naches, Washington, USA

R. Kwok
Jet Propulsion Laboratory, Pasadena, California, USA

R. Robins and M. Coon
NorthWest Research Associates, Inc., Bellevue, Washington, USA

Received 22 October 2004; revised 10 February 2005; accepted 24 March 2005; published 27 May 2005.

[1] High-resolution radar imagery shows that the dynamic response of winter sea ice to gradients in large-scale surface wind stress is often localized along quasi-linear fractures hundreds of kilometers long. Relative shearing motion across these narrow fractures can exceed 10 cm s^{-1}. In one event recorded during the drift of the SHEBA ice camp, we observed an intense zone of pycnocline upwelling (~14 m) associated with significant shear motion near the camp, while upward turbulent heat flux in the ocean boundary layer reached nearly 400 W m^{-2}, an order of magnitude greater than at any other time during the year-long drift. We attribute the upwelling to Ekman pumping associated with concentrated ice shear. Over the entire Arctic Ocean sea ice cover, this process could be responsible for significant heat exchange between the cold surface layer and warmer subsurface water at the ubiquitous fractures resulting from large-scale atmosphere-ice interactions. **Citation:** McPhee, M. G., R. Kwok, R. Robins, and M. Coon (2005), Upwelling of Arctic pycnocline associated with shear motion of sea ice, *Geophys. Res. Lett.*, *32*, L10616, doi:10.1029/2004GL021819.

1. Background

[2] The centerpiece of the 1997–1998 Surface Heat Budget of the Arctic (SHEBA) project was a scientific research station supported by icebreaker that drifted through an annual cycle in perennial sea ice in the Pacific sector of the Arctic Ocean north of Alaska [*Uttal et al.*, 2002]. A primary objective of SHEBA was to measure the energy components that determine the cycle of sea ice growth and decay, motivated by numerical climate simulations that show amplified response to climate warming in the Arctic [e.g., *Rind et al.*, 1995]. The simulations, which are sensitive to sea-ice feedback mechanisms, are consistent with mounting evidence that the extent and thickness of the Arctic ice pack are decreasing rapidly [*Rothrock et al.*, 1999; *Parkinson et al.*, 1999].

[3] Heat exchange between the ocean and sea ice plays an important, but enigmatic, role in the ice energy budget [*Maykut and Untersteiner*, 1971]. Over much of the Arctic, the relatively fresh Arctic Surface Layer (ASL) overlies a cold halocline that insulates the surface from the underlying warmer and saltier Atlantic Water. The density contrast at the base of the ASL presents a strong barrier to upward mixing by turbulence, hence most of the ocean heat flux in the central basins derives from solar heating through open leads and thin ice during summer, rather than from turbulent mixing of heat from below [*Maykut and McPhee*, 1995; *Perovich and Elder*, 2002]. Since most of the turbulent energy for mixing originates at the surface from ice motion,

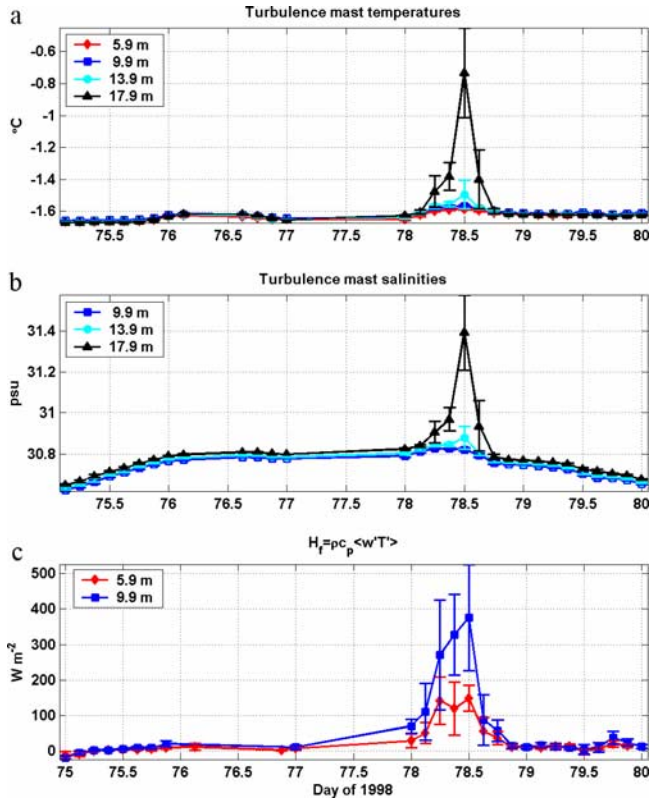

Figure 1. (a) Temperature (3-h averages) at fixed levels on the SHEBA turbulence mast. Error bars are twice the sample standard deviation. (b) Salinity. Conductivity measurements at 5.9 m were made with an open electrode microstructure instrument (c) Turbulent heat flux from the covariance of temperature deviations and vertical velocity. Error bars are twice the standard deviation of the 15-min turbulence realizations in each 3-h average. On day 78, clusters at 13.9 and 17.9 m were in the pycnocline where turbulence statistics were contaminated by internal waves.

0094-8276/05/2004GL021819

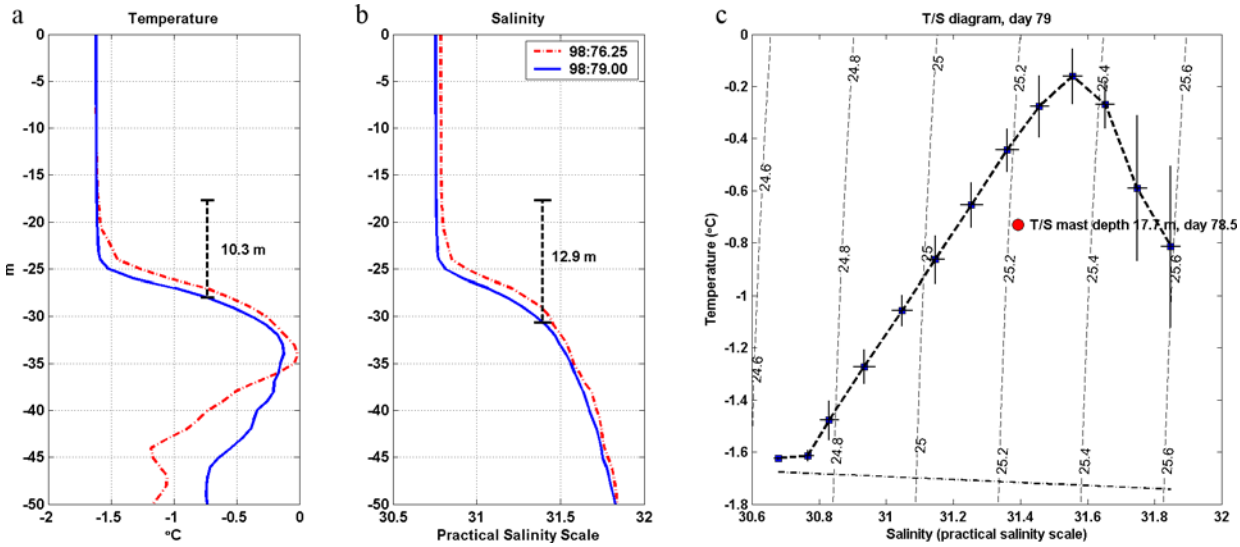

Figure 2. (a) Three-hour average temperature and (b) salinity profiles bracketing the period when the SHEBA profiling CTD was down for lack of ship power. Dashed vertical lines represent displacements of the isotherm and isohaline levels to the values observed at 17.9 m at time 78.5 (from Figure 1) (c) Average temperature/salinity characteristics from all CTD profiles on day 79. Dashed curves are potential density minus 1000 in kg m^{-3}. The solid circle shows *T*/*S* properties at 17.9 m at time day 78.5.

a physical process that raises the pycnocline will enhance heat exchange between the ASL and deeper water.

[4] Though mean circulation over the deep Canada Basin is sluggish, the halocline itself is fairly energetic, with numerous eddies (or submesoscale coherent vortices [SCVs]) [*D'Asaro*, 1988] with horizontal scales comparable to the internal Rossby deformation radius, typically 12 km [*Manley and Hunkins*, 1985]. Normally the SCVs are confined to the stable halocline between the ASL and the Atlantic layer, with little impact on the surface energy budget. Many exhibit temperature/salinity (*T*/*S*) properties in their core that differ from the ambient surroundings, often taken as evidence that they originated elsewhere, e.g., near the peripheral shelf breaks. Nevertheless, disturbances within the pycnocline, particularly those that interact with the ASL, are of much interest and are potentially important in the surface heat budget.

2. Measurements

[5] We measured the response of the upper ocean to surface stress from wind forced ice motion in order to gauge the energy exchange between the ice cover and underlying ocean. Ocean measurements included continuous mean velocity, temperature, salinity and turbulent fluxes at fixed levels in the ocean boundary layer (OBL) beneath the 2-m thick pack ice, plus a profiling conductivity/temperature/depth (CTD) instrument that cycled between the surface and 150 m depth at approximately 15-min intervals.

[6] Except for a few weeks in summer [*Perovich and Elder*, 2002; *McPhee et al.*, 2003], basal heat flux from the ocean boundary layer to the ice undersurface was modest, typically less than 5 W m^{-2}. There were occasional bursts to as much as 30 W m^{-2} in the OBL during storms, when heat from the pycnocline below the well mixed layer was mixed upward by turbulence. On March 19, 1998 (day 1998:78) turbulent heat flux measured near the top of the OBL (Figure 1) reached levels nearly an order of magnitude greater than at any other time during the year-long experiment. The event coincided with a dramatic manifestation of ice shear late in the afternoon (local time, UT-9 h) on Mar 18, when the ice floe on the ship's starboard shifted several hundred meters forward over the span of a few hours. An opening lead between the ship and experiment sites on the ice floe had earlier halted the profiling CTD program when the main power cable was severed; hence there were no continuous temperature and salinity profiles available on day 78. The inverted turbulence mast continued operating with power from a portable generator, and the profiler resumed operation on day 79.

[7] Time series of *T* and *S* at fixed levels compared with CTD profiles at times bracketing the cycling profiler data gap (Figure 2) indicate upwelling of relatively warm and saline pycnocline water on day 78. Vertical bars indicate displacements of the temperature and salinity values observed at 17.9 m on the fixed level mast at the time of peak upwelling (day 78.5) relative to typical ambient levels measured by the profiler 12 h later. The apparent isohaline displacement (approximately the same as the isopycnal displacement) is larger than the isothermal displacement by about 2.6 m, indicating preferential upward mixing of heat relative to salt during the energetic mixing event on day 78; i.e., a local mechanism for substantially changing *T*/*S* properties in the Arctic pycnocline (Figure 2c).

[8] Horizontal shear in ice velocity induces vertical motion at the base of the ASL by a mechanism called Ekman pumping. A rough approximation of the vertical velocity at the base of the boundary layer (w_p) is obtained by integrating the steady-state momentum equation from there to the ice/water interface [*Gill*, 1982]:

$$w_p - w_0 \approx \frac{1}{f} \nabla \times \boldsymbol{\tau}_0 \qquad (1)$$

where $w_p - w_0$ is the velocity relative to the surface of an isopycnal surface just below the turbulent boundary layer; f is the Coriolis parameter; and $\nabla \times \boldsymbol{\tau}_0$ is the curl of kinematic stress at the ice/water interface. This results from satisfying continuity when there is a gradient in Ekman transport in the turbulent boundary layer, where the transport is typically almost perpendicular to the interfacial stress [*McPhee and Smith*, 1976]. Upwelling of the pycnocline follows if the stress curl is positive, i.e., induced by counterclockwise rotation in the ice velocity field relative to the underlying ocean in the northern hemisphere.

[9] For a more comprehensive view of the ice motion field in the region surrounding the ship, we have utilized a recently developed tool that promises to greatly increase our understanding of kinematics of the Arctic sea ice cover: automated tracking of common features in satellite-borne synthetic aperture radar (SAR) imagery. During SHEBA, the RGPS System [*Kwok*, 1998] provided close to daily estimates of the average ice velocity and deformation on a uniform 5 km grid over an approximately 200 km by 200 km area centered on the camp.

[10] An example of the velocity field derived from feature tracking in two RGPS scenes spanning the period from 1998:77.75 to 78.73 (Figure 3a) illustrates that during the wind event on day 78, there was significant horizontal shear in the north-south direction and backing in ice drift direction going from west to east. Note that in the interpolated color representation of ice speed, two boundaries separating rather distinct bands appear, running roughly northwest-southeast. The drift of SHEBA crosses the more southerly boundary. These boundaries are emphasized in an estimate of minimum ice/ocean stress curl (Figure 3b) from

$$\nabla \times \boldsymbol{\tau}_0 \geq \frac{\Delta \tau_{0y}}{\Delta x} - \frac{\Delta \tau_{0x}}{\Delta y} \tag{2}$$

where the differentials are approximated by differences over the grid scale $\Delta x = \Delta y = 5$ km. Kinematic ice/ocean stress ($\boldsymbol{\tau}_0 = |\boldsymbol{u}_{*0}|\, \boldsymbol{u}_{*0}$, where $\boldsymbol{u}_{*0}$ is friction velocity at the interface) was calculated as a function of ice velocity relative to underlying geostrophic ocean current by considering planetary boundary layer similarity and data relating ice velocity to various measures of ice/ocean stress [*McPhee*, 1990; *McPhee et al.*, 2003]. In this part of the Arctic, geostrophic flow is generally small and was neglected relative to ice velocities observed on day 78.

[11] A remarkable result from the stress curl analysis is that the zone of moderate-to-intense shear experienced locally at the SHEBA site extended for at least 200 km in a clearly identifiable arc from southeast to northwest. A similar zone occurred about 40 km north of SHEBA on the same day. In fact, such features are common in the RGPS shear analysis of SAR images over the entire Arctic Ocean ice cover in winter (Figure 3c) [*Kwok*, 2001]. This illustrates one aspect of air-sea interaction that is apparently unique to ice-covered oceans, namely a mechanism for concentrating gradients in Ekman transport across very small horizontal scales. Wind is the primary mover of pack

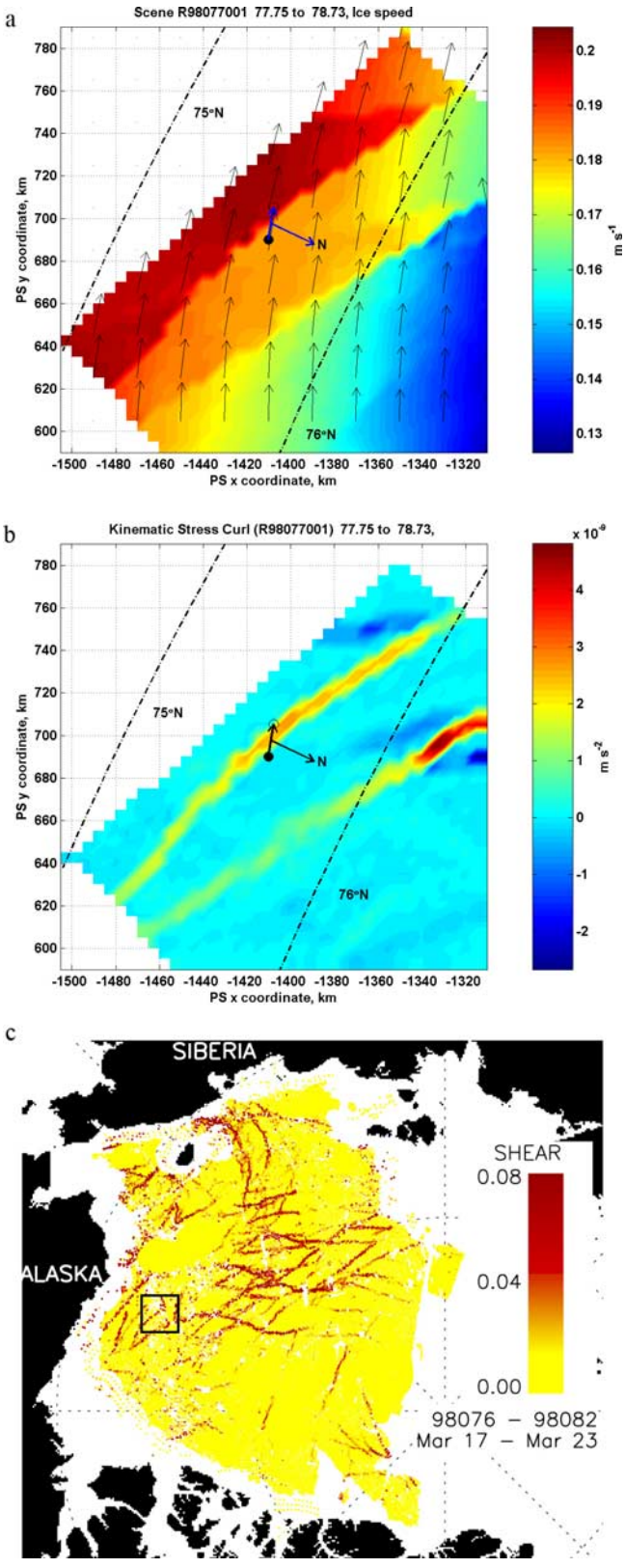

Figure 3. (a) Average velocity field from RGPS feature tracking in scenes separated by about one day. Circles show the beginning (solid) and ending (open) positions of the SHEBA drift station. Shading indicates ice speed; vectors show velocity at every 4th grid point. (b) Finite approximation of the kinematic ice/ocean stress curl derived from the velocity field (Figure 3a) with a grid spacing of 5 km. (c) Basin wide depiction of ice velocity shear from sequential SAR images for the week of Mar 17–23, 1998. Outlined box indicates the domain of Figures 3a and 3b.

ice in the Arctic, and in many situations the surface stress imposed by the wind is passed through to the upper ocean with only minor modification. But whereas changes in surface velocity and surface stress over the open ocean reflect the scale of the forcing atmospheric pressure fields (hence are often large compared with the ocean internal deformation radius), the mechanical properties of sea ice apparently localize these differences into relatively intense zones of surface vorticity (closely related to stress curl). This provides a plausible explanation for the anomalous upper ocean characteristics observed on March 19. Kinematic stress curl evaluated at the mean position of the ship in Figure 3b (about 2.3×10^{-9} m s^{-2}) most likely represents an underestimate of the actual value. Analysis of SAR images in the vicinity of the ship suggested that the width of the shearing lead closest to the station was 350 ± 100 m, an order of magnitude smaller than the grid size used in (2). Assuming that in actuality the velocity difference occurs over a scale of about 0.5 km, then integrating (1) over the one-day interval between RGPS scenes yields a pycnocline displacement of about 14 m, similar to the pycnocline displacement observed on day 78.

3. Discussion

[12] We cannot out of hand dismiss the possibility that the pycnocline disturbance observed on day 78 was an already existing SCV over which we fortuitously drifted during a time of significant ice deformation. However, two factors argue against this interpretation, and suggest instead that the feature had been generated recently in the near vicinity. First, there was strong turbulent mixing at the boundary between the ASL and halocline on day 78. Had the feature existed long enough to have migrated from some distance off, it would have had to survive several storms of equal or greater strength, in the face of intense turbulent diffusion. Second, the upper bound of its half-width scale (as inferred from our drift across it) was approximately 6 km, considerably smaller than the first-mode internal Rossby deformation radius in the Arctic (10–20 km). Under these conditions, buoyancy dominates rotation in the momentum balance [*Gill*, 1982]; thus the effects of friction, gravity, and rotation would combine to rapidly modify such a feature via the Rossby adjustment process [*Stern*, 1975].

[13] It is worth noting that the departure in *T*/*S* properties of the upwelled water from ambient conditions (circle symbol in Figure 2c), which we tentatively identify as resulting from different diffusion rates for heat and salt in the upper pycnocline, is comparable to the anomalous *T*/*S* properties observed in some Arctic SCVs [*Manley and Hunkins*, 1985]. By this apparent double-diffusive mechanism, a water parcel upwelled in the upper pycnocline can lose buoyancy, even if it retains its salinity characteristics, and it will seek a level lower in the water column after the upwelling event relaxes toward its initial state.

[14] Because of limited data availability caused by local ice deformation at the SHEBA site, it is difficult to interpret unequivocally the origin and fate of the anomalous upwelling event observed on day 78. Nevertheless, there is strong indication from the RGPS analysis that a mechanism whereby the ice cover concentrates gradients in the forcing wind field into narrow bands of intense shear, can induce major shifts in the elevation of the pycnocline, or equivalently the thickness of the well mixed ASL. The phenomenon would thus appear to be unique to ice covered oceans where the pack ice strength is sufficient to transfer stress over large distances. Our turbulence measurements indicate that such events may greatly enhance ocean-to-ice heat transfer locally, a conclusion corroborated by measurements of ice thickness at several locations on the SHEBA floe showing significant basal melting during late March. Normally, at that point in the seasonal cycle, the ice column is approaching its lowest temperature and is growing. Our local measurements, combined with the satellite imagery showing that intense shear zones are fairly common, suggest that the upwelling events may significantly impact the total surface heat budget. By preferential turbulent mixing of heat versus salt, they also provide a means of changing the *T*/*S* characteristics of upper pycnocline water. Finally, we conjecture that what are essentially line sources of vorticity hundreds of kilometers long (apparently a ubiquitous feature of the Arctic ice pack in winter (Figure 3c)) may induce longer lived pycnocline circulations by a mechanism not heretofore considered.

[15] **Acknowledgments.** We thank P. Lelong and M. Pruis for assistance with calculations, and critical reading of the draft manuscript. Support for this research by NASA and NSF OPP is gratefully acknowledged.

References

D'Asaro, E. A. (1988), Observations of small eddies in the Beaufort Sea, *J. Geophys. Res.*, *93*, 6669–6684.

Gill, A. E. (1982), *Atmosphere-Ocean Dynamics*, 661 pp., Elsevier, New York.

Kwok, R. (1998), The RADARSAT geophysical processor system, in *Analysis of SAR Data of the Polar Oceans: Recent Advances*, edited by C. Tsatsoulis and R. Kwok, pp. 235–257, Springer, New York.

Kwok, R. (2001), Deformation of the Arctic Ocean sea ice cover: November 1996 through April 1997, in *Scaling Laws in Ice Mechanics and Dynamics*, edited by J. Dempsey and H. H. Shen, pp. 315–323, Springer, New York.

Manley, T. O., and K. L. Hunkins (1985), Mesoscale eddies of the Arctic Ocean, *J. Geophys. Res.*, *90*, 4911–4930.

Maykut, G. A., and M. G. McPhee (1995), Solar heating of the Arctic mixed layer, *J. Geophys. Res.*, *100*, 24,691–24,703.

Maykut, G. A., and N. Untersteiner (1971), Some results from a time-dependent thermodynamic model of sea ice, *J. Geophys. Res.*, *76*, 1550–1575.

McPhee, M. G. (1990), Small scale processes, in *Polar Oceanography*, edited by W. Smith, pp. 287–334, Elsevier, New York.

McPhee, M. G., and J. D. Smith (1976), Measurements of the turbulent boundary layer under pack ice, *J. Phys. Oceanogr.*, *6*, 696–711.

McPhee, M. G., T. Kikuchi, J. H. Morison, and T. P. Stanton (2003), Ocean-to-ice heat flux at the North Pole environmental observatory, *Geophys. Res. Lett.*, *30*(24), 2274, doi:10.1029/2003GL018580.

Parkinson, C. L., D. J. Cavalieri, P. Gloersen, H. J. Zwally, and J. C. Comiso (1999), Arctic sea ice extents, areas, and trends, 1978–1996, *J. Geophys. Res.*, *104*, 20,837–20,856.

Perovich, D. K., and B. Elder (2002), Estimates of ocean heat flux at SHEBA, *Geophys. Res. Lett.*, *29*(9), 1344, doi:10.1029/2001GL014171.

Rind, D., R. Healy, C. Parkinson, and D. Martinson (1995), The role of sea ice in 2 × CO_2 climate model sensitivity. Part I: The total influence of sea ice thickness and extent, *J. Clim.*, *8*, 449–463.

Rothrock, D. A., Y. Yu, and G. A. Maykut (1999), Thinning of the Arctic ice cover, *Geophys. Res. Lett.*, *26*, 3469–3472.

Stern, M. E. (1975), *Ocean Circulation Physics*, 246 pp., Elsevier, New York.

Uttal, T., et al. (2002), The surface heat budget of the Arctic Ocean (SHEBA), *Bull. Am. Meteorol. Soc.*, *83*, 255–275.

M. Coon and R. Robins, NorthWest Research Associates, Inc., Bellevue, WA 98009, USA. (max@nwra.com)

R. Kwok, Jet Propulsion Laboratory, Pasadena, CA 91109, USA.

M. G. McPhee, McPhee Research Company, Naches, WA 98937, USA.